Sulfonated Poly(ether sulfone)/Phosphotungstic Acid/Attapulgite Composite Membranes for Direct Methanol Fuel Cells

Sheng Wen,[1,2] Chunli Gong,[2] Yao-Chi Shu,[3] Fang-Chang Tsai,[1] Jen-Taut Yeh[1,4,5]

[1]*Faculty of Materials Science and Engineering, Hubei University, Wuhan 430062, People's Republic of China*
[2]*Faculty of Chemistry and Material Science, Xiaogan University, Xiaogan, Hubei 432100, People's Republic of China*
[3]*Department of Polymer Materials, Vanung University, Tao-Yuan, Taiwan 32045, People's Republic of China*
[4]*Department and Graduate School of Polymer Engineering, National Taiwan University of Science and Technology, Taipei, Taiwan*
[5]*Key Laboratory of Green Processing and Functional Textiles of New Textile Materials (Wuhan University of Science and Engineering), Ministry of Education, Wuhan, People's Republic of China*

Received 28 August 2010; accepted 20 March 2011
DOI 10.1002/app.34540
Published online 28 July 2011 in Wiley Online Library (wileyonlinelibrary.com).

ABSTRACT: Novel composite sulfonated poly(ether sulfone)(SPES)/phosphotungstic acid (PWA)/attapulgite (AT) membranes were investigated for direct methanol fuel cells (DMFCs). Physical–chemical properties of the composite membranes were characterized by FTIR, DSC, TGA, SEM-EDX, water uptake, tensile test, proton conductivity, and methanol permeability. Compared with a pure SPES membrane, PWA, and AT doping in the membrane led to a higher thermal stability and glass transition temperature (T_g) as revealed by TGA and DSC. Tensile test indicated that lower AT content (3%) in the composite can significantly increase the tensile strength, while higher AT loading demonstrated a smaller contribution on strength. Proper PWA and AT loadings in the composite membranes can increase the proton conductivity and lower the methanol cross-over. The proton conductivity of the SPES-P-A 10% composite membrane reached 60% of the Nafion 112 membrane conductivity at room temperature while the methanol permeability was only one-fourth of that of Nafion 112 membrane. This excellent performances of SPES/PWA/AT composite membranes could indicate a potential feasibility as a promising electrolyte for DMFC.
 J Appl Polym Sci 123: 646–656, 2012

Key words: sulfonated poly(ether sulfones); composite membrane; methanol permeability; proton conductivity

INTRODUCTION

There is a growing interest over the past few years in the development of direct methanol fuel cells (DMFCs) due to their potential applications in portable devices and vehicles.[1–5] One of the main components in DMFCs is the electrolyte membrane which mainly serves as proton carrier and methanol obstructor. Dupont Nafion® or other perfluorinated sulfonic acid membranes are widely acknowledged to be good electrolyte membranes because of their high proton conductivity and chemical stability. However, Nafion® membranes have some drawbacks[6,7]: (i) Nafion® is too expensive and difficult to process; (ii) there is a strong dependence on relative humidity in maintaining the proton conductivity of Nafion® membranes. This is the reason why proton conductivity decreases with the dehydration at high temperature; (iii) thermal instability at high temperature. This property causes the membrane to physically shrink during high temperature operation, with subsequent poor contact and proton conductivity between the membrane and the electrodes; (iv) high methanol permeability, which not only wastes fuel but also reduces cell performance for application in DMFCs.

Contemporary electrolyte membrane research involves the development of new polymer electrolytes that are based on hydrocarbon polymers.[8] Among the potential alternatives, sulfonated poly (ether sulfone) (SPES) have attracted considerable attentions because of their excellent performance of film forming, low cost, easy preparation, good mechanic strength, and high chemical and thermal stabilities.[9–14] However, similar to other sulfonated aromatic polymers, SPES should possess high sulfonation level to achieve sufficient proton conductivity because the acidity of the SPES is lower than that of the perfluorosulfonic acid under the same sulfonation level. Unfortunately, the increase in the concentration of sulfonated groups in the membranes is responsible for poor mechanical properties and

Correspondence to: J.-T. Yeh (jyeh@tx.ntust.edu.tw).
Contract grant sponsor: Hubei Provincial Department of Education; contract grant number: Q20102704.

excessive methanol cross-over. To balance the relationship among proton conductivity, mechanic strength and methanol cross-over, organic/inorganic composite membranes have become an interesting topic in DMFCs researches.[15–19]

Phosphotungstic acid (PWA) is one of the heteropolyacids (HPA) that are attractive inorganic additives because of their high proton conductivity and thermal stability in crystalline form.[19,20] Fenton and coworkers[21] recast the Nafion/HPA composite for H_2/O_2 fuel cell and found that the HPA can increase the conductivity of the membrane. Staiti et al.[22] and Shao et al.[23] evaluated PWA-doped composite silica/Nafion/PWA membranes for high-temperature DMFCs (145°C). Kim et al.[24] have studied the composite membranes of PWA and sulfonated poly (arylene ether sulfone), and achieved the proton conductivity of 0.15 S/cm. However, although PWA can increase proton conductivity of membranes to some extent, the resistance of membranes for methanol diffusion is not improved. It is well known that the layered clay such as montmorillonite (MMT) can provide excellent barrier effect for the permeation of small molecules.[17,25] In our study, another clay that is different from MMT, attapulgite (AT) is adopted and filled in the SPES/PWA system. AT is a family of fibrous hydrous magnesium aluminum silicates with unique three-dimensional structure. AT has the structural formula $Mg_5Si_8O_{20}(OH_2)_2(OH)_4{\cdot}4H_2O$ and has a large surface area and strong absorptive capacity.[26–28] In addition, it has good mechanical strength and thermal stability. So in this work, we try to maintain low methanol permeability and high proton conductivity with the incorporation of AT and good proton conductor of PWA. The SPES/PWA/AT composite membranes with various PWA and AT loadings were prepared. The morphologies and properties, including the thermal and tensile properties, water uptake, proton conductivities, and methanol permeability, have been varied by the variation of the composition of the composite membrane.

EXPERIMENTAL

Sulfonation of PES

Sulfonation of PES (Ultrason® E6020P, T_g = 225°C, M_w = 51 kg/mol, M_w/M_n = 3.5, BASF corp.) was carried out in a concentrated sulfuric acid (98%) solvent using chlorosulfonic acid as a sulfonating agent following the procedure described by Dai et al.[29] The ion exchange capacity (IEC) value of SPES was determined by the acid–base back titration method according to known references.[13,20] SPES membrane samples were soaked in a 1*M* NaCl solution for at least 48 h. Thus, the protons of the sulfonic acid groups were exchanged with sodium ions. Then the exchanged protons were titrated with 0.01*M* NaOH solution with phenolphthalein as an indicator. The titrated IEC was determined from formula:

$$\mathrm{IEC} = \frac{C \times V}{M} \times 100 \quad (1)$$

where C was the concentration of NaOH, V the volume of NaOH, and M was the weight of the membrane.

The corresponding degree of sulfonation (DS) was calculated as following equation:

$$\mathrm{IEC} = \frac{1000\mathrm{DS}}{232 + 81 \times \mathrm{DS}} \quad (2)$$

where 232 and 81 are the molecular weights of the PES unit and the sulfonic acid group, respectively. In this article, the IEC of the obtained SPES was 1.34 meq/g, that is, DS was 35%.

Preparation of composite membranes

SPES was dissolved in DMAc to form a 10 wt % transparent solution, PWA (AR, Sinopharm Chemical Reagent Co., China) and AT (AR, GEL-2, Huaiyuan Mining Industry Co., Jiangsu Province, China) (weight ratio of PWA:AT = 2 : 5) were added into the SPES solution. The formed solution was stirred with a magnetic stirrer for 1 h and degassed by ultrasonication. The content of AT in the mixture were varied in 3, 5, 10, and 15 wt % based on SPES. To remove any impurities, the casting solutions were filtered through a 0.2-mm pore size Teflon filter before membrane preparation. The prepared mixture was slowly poured into a glass dish in an amount that would give a thickness of ~60 μm of the formed composite membrane. The procedure of membrane-drying involved air-drying at 80°C for 4 h, followed by 120°C for 12 h, and then drying under vacuum at 120°C for 24 h. Hereafter, the notations of composite membranes are denoted as SPES-P-A x, where x is the weight percentage of AT in the SPES matrix.

FTIR

FTIR spectra were obtained by using a Nicolet 380 Fourier transform spectrometer with a resolution of 2 cm^{-1}.

Differential scanning calorimetry (DSC)

The glass transition temperatures were obtained with a Perkin–Elmer DSC-7 differential scanning calorimeter. Scans were conducted under nitrogen by

heating up to 220°C, annealing at 220°C for 10 min to eliminate the prior thermal and solvent histories, and then quenching quickly to room temperature. A DSC heating experiment was performed at 10°C/min to measure T_g. The T_g values are reported as midpoints of the changes in the slope of the baseline.

Thermogravimetric analysis

Thermogravimetric analysis (TGA) of membranes was obtained by TGA (TA SDT-Q600) in a nitrogen atmosphere at a heating rate of 10°C/min over the range 25–700°C. The TGA outlet was coupled online with a Nicolet 380 FTIR spectrometer through a gas cell, which was warmed up to 240°C and stabilized for 2 h before performing TGA.

X-ray diffraction (XRD)

XRD experiments were performed on a Rigaku X-ray automatic diffractometer D/max-IIIc (Japan). The dried membranes were mounted on an aluminum sample holder. The scanning angle ranged from 3° to 60° with a scanning rate 3°/min and with a step size of 2θ equal to 0.05°.

Morphology

The cross-section of the membranes was examined using a scanning electron microscope (SEM) X-650 from HITACHI equipped with an energy dispersive X-ray (EDX) spectrometer. The membranes were fractured by brief immersion in liquid nitrogen. Fresh cross-section cryogenic fractures of the membranes were vacuum-sputtered with a thin layer of Pt/Pd prior to analysis.

Water uptake

The composite membranes were dried in a vacuum oven at 100°C for 24 h, weighed (W_{dry}), and immersed in deionized water at different temperature for 48 h. Then, the wet membranes were blotted to remove surface water droplets and quickly weighed (W_{wet}). The water uptake of membranes was calculated as follows:

$$\text{Water uptake } (\%) = \frac{W_{wet} - W_{dry}}{W_{dry}} \times 100\% \quad (3)$$

PWA extraction

The amount of PWA extracted from the composite membranes was determined by weight loss according to the procedure described by Wang et al.[30] and Choi et al.[31] The membranes were first dried in a vacuum oven at 100°C for 24 h. After drying, the membranes were weighed to obtain an initial weight. They were then immersed in deionized water at room temperature for 24 h, followed by immersing in boiling water for another 24 h. The membranes were finally dried in a vacuum oven at 100°C for 24 h and weighed again. The PWA extraction values were recorded as a weight loss percentage.

Tensile test

The dumbbell specimens were measured with tension tester (GT-TFS2000, Gotech testing machines, Taiwan) at a cross-head speed of 2 mm/min at room temperature. The gauge length and width of dumbbell specimens were 50 mm and 4 mm, respectively. At least three specimens were tested for each sample and then averaged.

Proton conductivity measurements

The proton conductivity in water-equilibrated membranes was measured using the AC impedance technology. The impedance measurement was carried out by Solatron 1260 impedance analyzer over the frequency range from 0.1 Hz to 10 MHz. Before the proton conductivity was measured, all membranes were hydrated by immersion in deionized water for 24 h at room temperature. A sample of prehydrated membrane (3 × 3 cm) was clamped between the two electrodes. The proton conductivity was calculated as follows:

$$\sigma = l/Rdw \quad (4)$$

where l is the distance between the electrodes; d and w are the thickness and width of the films, respectively, and R is the resistance value measured.

Methanol permeability

Measurement of methanol permeability was carried out using a two-compartment cell as described in our previous work.[16,32]

Initially one compartment B of the cell (V_B = 20 mL) was filled with 0.2 vol % ethanol solution in deionized water. The other compartment A (V_A = 20 mL) was filled with 8 vol % methanol and 0.2 vol % ethanol and deionized water. The membrane with the diffusion area of 3.14 cm^2 sandwiched by O-ring shape Teflon was clamped between the two compartments. The membrane samples were equilibrated in deionized water for 24 h before testing. The diffusion cell was kept stirring slowly during experiment. The solution samples (about 2 μL) in

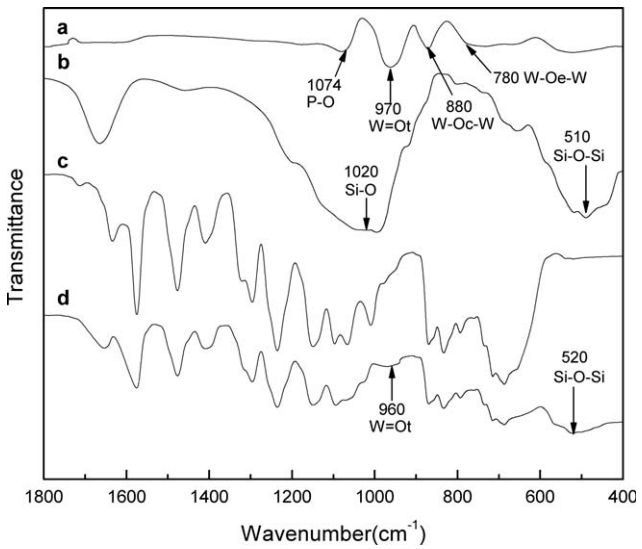

Figure 1 FTIR spectra of line (a) PWA; line (b) AT; line (c) pure SPES; line (d) SPES-P-A 10%.

compartment *B* were taken at interval and were analyzed by gas chromatography (GC-5890 series*II*, Hewlett–Packard) using HP-20*M* (CARBOWAX 20*M* phase) chromatographic column together with a flame ionization detector. Methanol permeability was calculated by following equation:

$$C_B = \frac{D \times K \times C_A \times A}{V_B \times L} \times t \tag{5}$$

where C_B is the methanol concentration in compartment *B*, C_A is the methanol concentration in compartment *A*, *A*, *L*, and V_B are the diffusion area of membrane, the thickness and the solution volume of compartment *B*. *D*, *K*, and *t* are the methanol diffusivity, the solubility, and the permeability time, respectively. The methanol permeability (P_m) is defined as the product of diffusivity and solubility (DK).

RESULTS AND DISCUSSION

FTIR analysis

Figure 1 shows the FTIR spectra for the PWA, AT, the pure SPES film and the SPES-P-A composite membranes, respectively. Neat PWA exhibited absorption bands at 1074, 970, 880, and 780 cm^{-1}, attributed to the stretching vibrations of P—O, W=O_t (O_t is the terminal oxygen), W—O_c—W (corner-shared octahedral), and W—O_e—W (edge-shared octahedral), respectively.[31] As shown in Figure 1(b), the broad absorption band at 1020 cm^{-1} was assigned to the Si—O stretching vibration and Si—O—Si deformation vibration was in the $\sim$ 510 cm^{-1}. Two characteristic peaks at 1066 cm^{-1} and 1025 cm^{-1} were assigned to the symmetric and asymmetric stretches of the sulfonated groups of SPES. The peaks at 1362 cm^{-1}, 1237 cm^{-1}, and 1275 cm^{-1} were attributable to the aromatic ether νC—O—C. The stretching vibrations of the aromatic ring bone were in the 1446–1630 cm^{-1} wave band. After incorporation of PWA and AT, the obvious absorption bands at 960 and 520 cm^{-1} in the SPES-P-A 10% composite are contributed to the W=O_t stretching and Si—O—Si deformation vibrations. FTIR result indicates that PWA and AT has been successfully incorporated into the SPES polymer matrix.

Glass transition temperature

The DSC measurements were carried out by a heating-cooling-heating cycle. The purpose of the first heating cycle was to remove any thermal history of the composite membrane. The DSC (2nd heating) curves for the pure SPES membrane and SPES-P-A composite membrane with various PWA and AT compositions are shown in Figure 2. The glass transition temperatures (T_g) of pure SPES membrane and all SPES-P-A composite membranes are also listed in Table I. Apparently, the T_g increased for the composite membranes, which implied that they were thermomechanically more stable than the pure SPES membrane. For instance, the T_g for SPES was determined to be around 220°C, whereas for SPES-P-A 5%, SPES-P-A 10%, SPES-P-A 15% composite membranes, the temperatures shifted to about 233, 241, and 245°C, respectively. The increment of T_g is attributed to the specific interactions between the sulfonic acid groups in polymer chains, PWA and AT. This conclusion was also in agreement with the TGA thermograms, which showed an increase in the

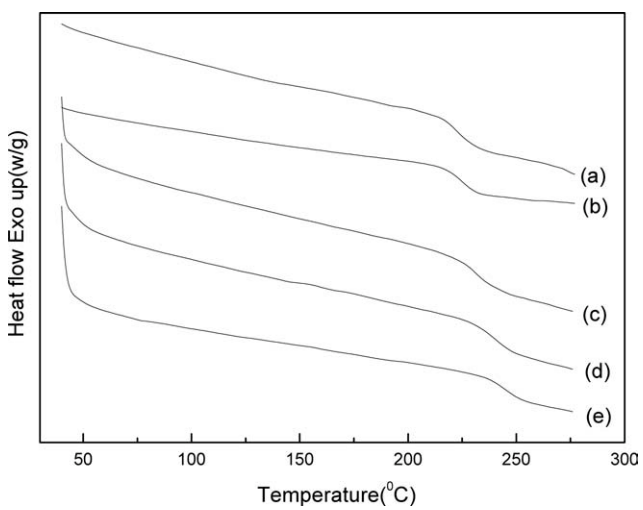

Figure 2 DSC curves of (a) SPES, (b) SPES-P-A 3%, (c) SPES-P-A 5%, (d) SPES-P-A 10%, and (e) SPES-P-A 15%.

TABLE I
T_g and Tensile Properties of Nafion 112 and the Composite Membrane

Samples	T_g (°C)	Young's modulus (MPa)	Tensile strength (MPa)	Elongation (%)
SPES	223	860.2	43.73	21.09
SPES-P-A 3%	225	884.3	72.10	19.58
SPES-P-A 5%	233	916.5	61.75	17.22
SPES-P-A 10%	241	945.9	56.56	14.98
SPES-P-A 15%	245	1011.3	39.73	9.87
Nafion® 112	–	240.5	27.10	310

degradation temperatures for the composite membranes, as will be discussed later.

Thermal stability

The thermal stability of PWA, AT, pure SPES and the representative composite membrane was studied by TGA, as shown in Figure 3. The TGA curve of PWA shows a slight weight loss at about 150°C, probably because of dehydration of the water of crystallization, and then no further significant weight loss is observed until 700°C. For AT, a weight loss of ~ 8 wt % shown in Figure 3(b) was recorded between 50 and 150°C, and probably caused by the adsorbed water. The second weight loss, between 200 and 350°C, is believed to be associated with the loss of zeolite water in the AT. And the weight loss of AT in the temperature range from 400 to 550°C is related to the crystal water bonded by the cations in the octahedrons.[33,34]

As shown in Figure 3[(c,d) and (c′,d′)], the pure SPES and SPES-P-A composite membranes exhibit similar four-step degradation pattern, which appear as four major peaks in the DTG curves. In the first step, the weight loss begins below 100°C and continues up to 120°C. This step is followed in that order by three other degradation steps at ~ 180°C, 370°C and 440°C. The initial weight loss is caused by the removal of water from the hydrogroscopic samples. The second weight loss is observed in the temperature range 180 ~ 280°C, which is due to the residual DMAc solvent and water loss caused by the strong hydrogen bonding between the water molecules and the sulfonic acid groups in the samples. To verify this suppose, we used TGA-FTIR coupling technique to determine the FTIR spectra of gas escaping from the SPES-P-A 10% composite membrane at various temperatures. As shown in Figure 4 (240°C), The strong sharp peak at ~ 1680 cm^{-1}, which cannot be observed in the latter weight loss stage, is due to the characteristic absorption of the carbonyl group in DMAc. Meanwhile, the peak island appear at the ~ 2900 cm^{-1}(below 3000 cm^{-1}) suggest the cleavage of the alkyl chain and existence of saturated carbon hydrogen bonds that is only exist in the DMAc molecule. And the ~ 1390 cm^{-1} band, the symmetric bending vibration of —CH_3, also certifies the existence of the residual solvent in the membranes. As reported by our earlier work,[14] this phenomenon can be explained as follows: The boiling point of DMAc at atmospheric pressure is about 165°C, which is much less than the temperatures (180 ~ 280°C). However, at the temperature of the solvent boiling point, the composite materials are still in a glass state. The residual solvent cannot be removed completely from the composite membranes by heat treatment because of the solvent strongly bound to the polymer. When temperature is above 200°C, the hybrid materials are already in a rubbery state. An increase in the free volume in the rubbery state and the increased sliding of polymer chains with an

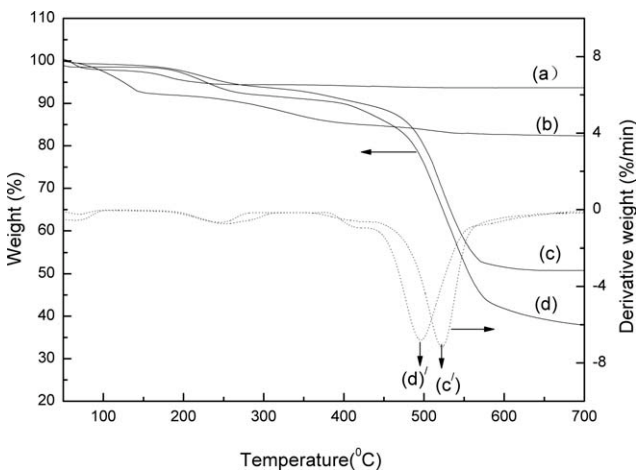

Figure 3 TGA diagrams of (a) PWA, (b) AT, (c) SPES-P-A 10%, (d) neat SPES and DTG curves of (c/) SPESP-A 10%, (d/) neat SPES.

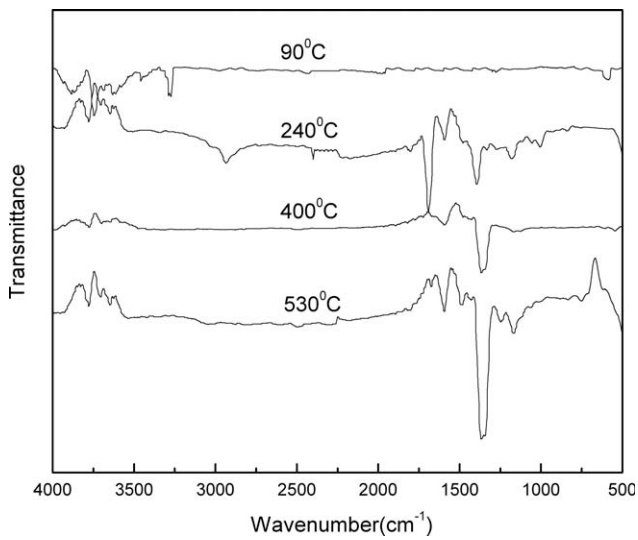

Figure 4 FTIR spectra of gas escaping from the SPES-P-A 10% composite membrane at different temperature.

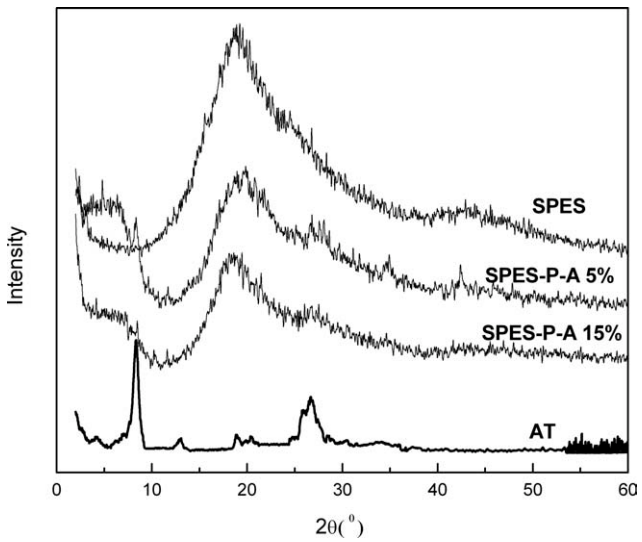

Figure 5 XRD patterns of AT, pure SPES, and SPES-P-A composite membranes.

increase in the temperature would enhance the evaporation of the residual solvent entrapped in the polymer in the glass state. The shoulder weight loss of neat SPES and SPES-P-A composite membranes, starting from $\sim 370^{\circ}C$, was recorded because the sulfonic acid groups were thermally decomposed through this region. This fact was verified by the FTIR spectrum of the decomposition gas of the SPES-P-A 10% composite membrane at 400°C. The $\sim$ 1365 cm^{-1} absorption peak indicates the existence of S=O segments. Although there are sulfone groups in the PES main chain, the other groups in the PES backbone were not detected in the gaseous products from the second weight loss. This thermal degradation range confirms the result reported by Guan et al.[35] And the last stage occurring at about 440°C is the splitting of the polymer main chains.

Furthermore, we can also notice that the degradation peaks of the SPES-P-A composite membrane are less intense and shift toward higher temperature. It can be concluded that the thermal stability is slightly improved probably due to the additive effect of PWA and AT fillers, indicating their suitability for high temperature PEMFC.

XRD patterns and SEM analysis

Figure 5 shows the XRD patterns of AT, pure SPES and the representative SPES-P-A composite membranes. As reported by Wang et al.,[28] the peaks at $2\theta = 8.3$, 13.6, 19.6, and 26.4° corresponded to the primary diffraction of the, (110), (200), (040), and (400) planes of the AT, respectively. As for the pure SPES, the scattering spectrum showed a broad scattering maxima and the major peak is located at 2θ around 18°, indicating that the SPES membrane samples was in the amorphous state. When PWA and AT were incorporated in the SPES matrix, the XRD patterns of the composites showed similar curves and indicates the absence of the representative crystalline peaks of AT, which were overlaid on a broad amorphous halo. However, we can notice that the main peak of SPES-P-A 15% shifted to lower 2θ value compared with that of the pure SPES sample. This indicates that the *d*-spacing was enlarged at high filler loading. And meanwhile, it is evident from Figure 5 that the value of intensity decreases with increasing PWA and AT content. For example, the value decreased from 472 CPS for pure SPES to 243 CPS for the SPES-P-A 15% composite. This result indicates less order of macromolecular orientation within the polymer after incorporation.

The cross-sections of PWA, AT, SPES, and composite SPES-P-A membranes were analyzed using SEM to observe the morphology and distribution of inorganic additives. As shown in Figure 6(c), the pure SPES membrane shows a very homogeneous and dense cross-section. On the other hand, the composite membranes show some very interesting features and exhibit a micro-phase separation inside the membranes. From Figure 6(d), we can clearly see that the AT in the membrane matrix has a fibrous morphology and its diameter is about 5 nm. With PWA and AT content increased, the fibrous morphology became to be hardly visible and while some small aggregates appeared in the composites, as shown in Figure 6(e,f). Figure 7(b) shows the EDX spectrum of the SPES-P-A10% membrane cross-section. For comparison, the EDX spectrum of the pure SPES also listed in Figure 7(a). It was the obvious evidence of existence of the PWA (P and W element) and AT (Si, Mg, and Al element). In the EDX mapping image, as shown in Figure 7(c,d), the Si and W elements are highlighted as bright dots. This image indicated a uniform distribution of fillers embedded throughout the sulfonated polymer matrix, although there was a little aggregated phenomenon in the composites.

Tensile properties

It is essential for PEMs to possess adequate mechanical strength under dry and humidified conditions. Here, the tensile test of membranes was conducted at ambient conditions with relative humidity (RH) $\sim$ 70%, and the results are listed in Table I. For comparison, the Nafion 112 membrane was also tested under the same conditions.

The Nafion 112 membrane showed a Young's modulus of 240.5 MPa, elongation at break 310%, and a maximum stress of 27.10 MPa, which are quite similar to the results from Nafion product information reported by DuPont[36] at similar ambient conditions. As for the

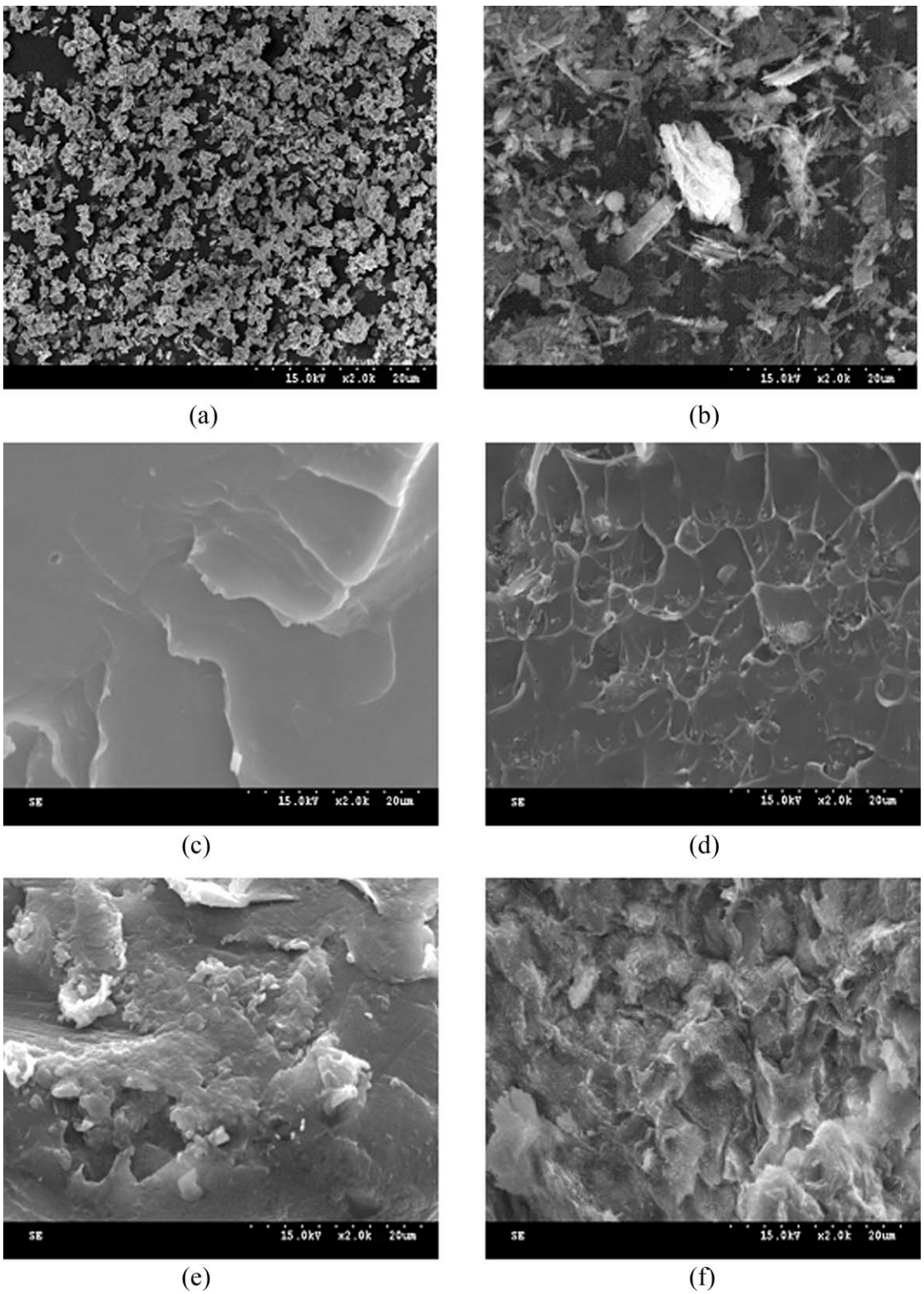

Figure 6 Cross-sectional SEM micrographs of the additives and composite membranes PWA, (b) AT, (c) SPES, (d) SPES-P-A 5%, (e) SPES-P-A 10%, (f) SPES-P-A 15%.

SPES-P-A composite membranes, the tensile strength increased from 43.73 to 72.10 Mpa with increasing AT loading from 0 to 3 wt % (PWA content from 0 to 1.2 wt %). However, a further increase in inorganic fillers did not contribute to any additional increase in tensile strength but declined the strength. For example, the tensile strengths of SPES-P-A 5%, -10%, and -15% composite membrane were 61.75, 56.56, and 39.73 Mpa,

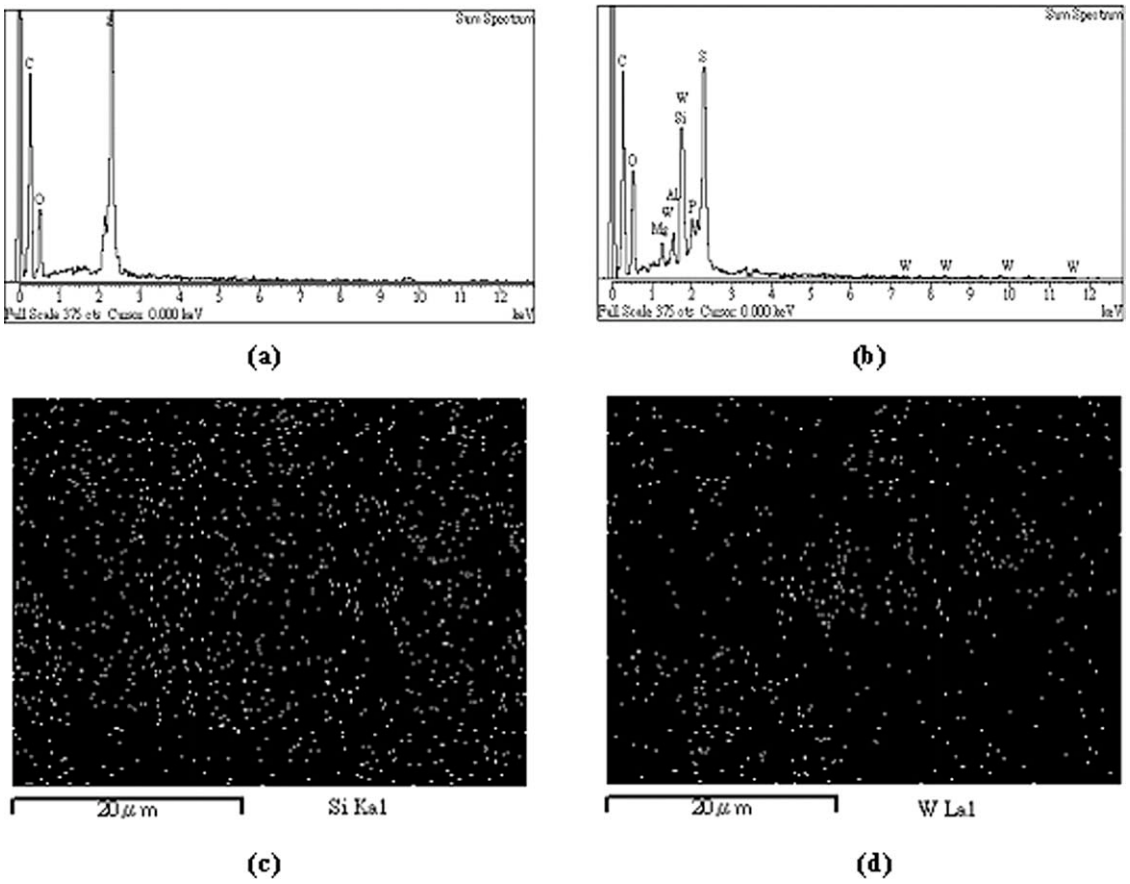

Figure 7 EDX measurement of the cross-section of (a) pure SPES, (b) SPES-P-A 10% composite membrane, and EDX mapping images for the elements (c) Si and (d) W of the SPES-P-A 10% cross-section.

respectively. This phenomenon could be explained as follows: at low PWA and AT loadings, the high strength and rigidity of the additives, which were dispersed very well in the polymer matrix, increased the tensile strength and Young's modulus of the composite membranes. As reported by Wang et al.,[28] at higher the inorganic additives loadings (especially the AT content), the AT would become the stress concentration points in the composite membranes due to the aggregation of AT, resulting the decrease of the tensile strength. In addition, a uniform decrease in the elongation of the composite membranes was seen in the ambient condition. The reason could be that the introduction of the inorganic additives into the sulfonated polymer damaged the ordering of the aggregative state. By increasing the additives content, the degree of order would decrease. The elongation at break of the composite membranes decreased from the 21.09% to 9.87% as AT increased from 0 to 15%.

We can also notice that although the tensile strength of the SPES-P-A composite membranes showed a decreased trend with higher PWA and AT loading, but the values of strength are higher than that of the Nafion 112 membrane. These data indicate that the composite membranes had adequate strength and could be used in PEMFCs.

Water uptake

Water uptake is closely related to the basic membrane properties and plays an essential role in the membrane behavior. The water within the membrane provides a carrier for the proton and maintains high proton conductivity. However, excessive water uptake in a PEM leads to unacceptable dimensional change or loss of dimensional shape, which could lead to weakness or a dimensional mismatch when incorporated into a membrane electrode assembly (MEA).[37,38] Moreover, higher swelling also leads to high methanol permeability. Hence optimization of water uptake and polymer swelling is required for the successful operation in a fuel cell.

Figure 8 displays the water uptake of the SPES-P-A composite membranes as a function of temperature. It can be seen that the water uptake of the pure SPES membrane was around 29% up to 60°C, increasing rapidly at higher temperature and was 42.6% at 100°C. Very high water uptake may lead to excessive swelling, which will result in loss of mechanical stability of membranes. Water uptake of composite membranes increased with the loading of PWA and AT increasing. This increase in water uptake can be attributed to the excellent hydrophilicity of AT. It is

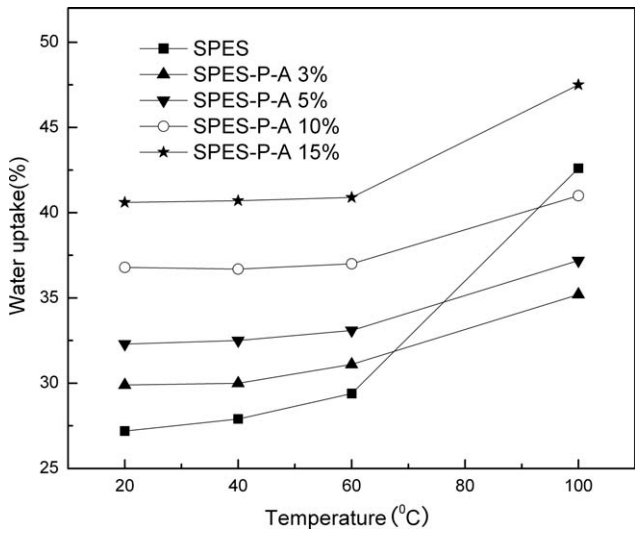

Figure 8 Water uptake of SPES and composite membranes.

known from the literature[27,28] that the surface of AT is covered with numerous Si—OH groups. Nevertheless, as temperature increased, the increasing trend of water uptake in the SPES-P-A composite membranes was lower than that in the pure SPES membrane. For examples, the water uptakes of SPES-P-A 3%, SPES-P-A 5%, and SPES-P-A 10% were 35.2%, 37.4%, and 41.0% at 100°C, respectively, which is less than that of SPES. This may be due to the cohesion of functional groups between SPES matrix, PWA and AT, which results in the generation of cross-link points, and then resist excessive swelling. These studies indicate that the composite membranes having less than 10% AT content (PWA content less than 4%) may maintain their mechanical integrity at higher temperatures and is worth investigating for practical applications.

PWA extraction

Because the PWA itself is a water soluble material, it would be easily extracted from the composite membrane in the presence of water. This extraction of HPA would lead to a decrease in proton conductivity and durable lifetime in fuel cell systems.[12] Thus, the retention of HPA was considered as one of the key parameters on determining the feasibility of the composite membranes used in the fuel cell systems. Table II lists the PWA extraction content of the composite membranes. It can be seen that the extraction of PWA from the composite membranes increased with the PWA content increased. It is interesting that the SPES membrane still had a weight loss, despite no PWA in the membrane. This weight loss in the SPES membrane might be due to the presence of residual solvent or some high boiling-point water-soluble impurities. This can be verified by the TGA results. As for the SPES-P-A composite membranes, the amount of PWA extraction increased from 0.6% to 1.5% when PWA content increased from 1.2 to 6%. However, they all showed a negligible PWA extraction. This low weight loss is probably because of the strong interaction of PWA with both the sulfonic acid groups in the SPES and hydroxyl groups in the AT.

Proton conductivity and methanol permeability

The proton conductivity is a decisive property for fuel cell membranes as the efficiency of the fuel cell depends on the proton conductivity. Generally, proton conductivity directly depends on the water uptake and IEC of the sulfonated polymer. Table II lists the results of proton conductivity at 20°C and 80°C, respectively. Obviously, the conductivity of all the membranes increased with increase in temperature. This phenomenon may be due to the increased mobility of water and structural reorientation as well as increased molecular mobility.[24] It can also be seen that proton conductivity increased with increasing amounts of AT up to a weight fraction of 10%. A maximum proton conductivity at room temperature of 0.030 S/cm was achieved for the SPES-P-A 10% composite membrane. This behavior can presumably be attributed to the following two factors: (1) the AT incorporated in composite membranes can absorb many water molecules. This water-rich surrounding enables the PWA to be an effective proton conductor; (2) the enhanced acidity of the sulfonic acid in the polymer matrix caused by PWA

TABLE II
IEC Values, PWA Extraction Amount, Proton Conductivity, and Methanol Permeability for the Composite Membranes

Samples	IEC (meq/g)	Weight loss (%)	Conductivity (S/cm) 20°C	Conductivity (S/cm) 80°C	Methanol permeability (cm^2/s)
SPES	1.34	0.3	0.0065	0.011	5.43×10^{-7}
SPES-P-A 3%	1.31	0.6	0.0092	0.017	5.05×10^{-7}
SPES-P-A 5%	1.28	0.8	0.021	0.039	4.78×10^{-7}
SPES-P-A 10%	1.22	1.1	0.030	0.047	2.55×10^{-7}
SPES-P-A 15%	1.17	1.5	0.024	0.040	1.08×10^{-7}
Nafion 112	0.92	–	0.051	0.090	1.05×10^{-6}

incorporation. Nevertheless, with the AT content above 10%, the proton conductivity decreased to some extent. For example, the proton conductivity decreased from 0.030 S/cm to 0.024 S/cm with AT increased from 10 to 15%. This phenomenon may be related to the nonconductive of the AT itself, and meanwhile, the loss of ionic sites (SO_3^-) because of the strong hydrogen bonding interaction between the sulfonic acid and the PWA molecules should also be responsible for the decrease of proton conductivity.

To prevent fuel waste and reduce catalyst poisoning and energy efficiency loss, the proton exchange membranes used in DMFCs should possess low methanol cross-over. The methanol permeability values of the composite membranes and Nafion 112 membrane at room temperature were measured and the results were listed in Table II. Compared with Nafion 112 membrane, all the SPES-P-A composite membranes including the pure SPES membrane had lower methanol permeability. Moreover, a continuous decrease of methanol permeability was discovered with increasing PWA and AT content in the composite membranes. In addition, it can also be noticed that the decline amplitude is not unchangeable. For example, as the AT content increased from 0 to 5%, the methanol permeability decreased from 5.43×10^{-7} to 4.78×10^{-7} cm^2/s; i.e., the decrease in amplitude is only 1.3×10^{-8} cm^2/s per percentage point of AT. However, when the AT content increase from 5 to 10%, the evident decrease in the amplitude is 4.46×10^{-8} cm^2/s per percentage point of AT. For the composite membrane with 15% AT, the methanol permeability is only 1.08×10^{-8} cm^2/s. This different decrease in methanol permeability may be caused by the formation of the massive or layered aggregates in the composites with high AT content, as discussed in SEM analysis. Hence, these aggregates can efficiently prevent methanol across the composite membranes.

CONCLUSIONS

The SPES/PWA/AT composite membranes with various PWA and AT loadings were prepared by solution blend method. The effect of PWA and AT on the properties of composite membranes was evaluated by thermal properties, water uptake, morphology, tensile properties, proton conductivity, and methanol permeability. The composite membranes showed higher thermal stability and T_g than the pure SPES membrane. Water uptake of the membranes was enhanced by incorporation of PWA and AT into SPES matrix. Tensile strength increased in the composite membranes with lower PWA and AT loadings (3% AT); higher AT (5–15% AT content) loadings presented a decrease in tensile strength. But even when the content of AT was as high as 15%, the composite membranes still possessed adequate strength for fuel cell application. The SPES-P-A 10% composite membrane showed highest proton conductivity (0.030 S/cm), which was 60% of the Nafion 112 membrane' conductivity. And especially, the methanol permeability of the composite membranes was very excellent. The excellent comprehensive property of the SPES-P-A composite membrane suggests their suitability as electrolytes in DMFCs applications.

The authors are grateful to BASF for kindly providing PES materials.

References

1. Rhee, C. H.; Kim, H. K.; Chang, H.; Lee, J. S. Chem Mater 2005, 17, 1691.
2. Hampson, N. A.; Wilars, M. J. J Power Sources 1979, 4, 191.
3. Wasmus, S.; Kuver, A. J Electroanal Chem 1999, 461, 14.
4. Dimitrova, P.; Friedrich, K. A.; Vogt, B.; Stimming, U. J Electroanal Chem 2002, 532, 75.
5. Jiang, R.; Kunz, H. R.; Fenton, J. M. J Membr Sci 2006, 272, 116.
6. Nagarale, R. K.; Gohil, G. S.; Shahi, V. K. J Membr Sci 2006, 280, 389.
7. Tsai, J. C.; Kuo, J. F.; Chen, C. Y. J Power Sources 2007, 174, 103.
8. Rikukawa, M.; Sanui, K. Prog Polym Sci 2000, 25, 1463.
9. Nolte, R.; Ledjeff, K.; Bauer, M.; Muhaupt, R. J Membr Sci 1993, 83, 211.
10. Koter, S.; Piotrowski, P.; Kerres, J. J Membr Sci 1999, 153, 83.
11. Wiles, K. B.; de Diego, C. M.; de Abajo, J.; McGrath, J. E. J Membr Sci 2007, 294, 22.
12. Miyatake, K.; Chikashige, Y.; Watanabe, M. Macromolecules 2003, 36, 9691.
13. Poppe, D.; Frey, H.; Kreuer, K. D.; Heinzel, A.; Mulhaupt, R. Macromolecules 2002, 35, 7936.
14. Wen, S.; Gong, C.; Tsen, W. C.; Shu, Y. C.; Tsai, F. C. Int J Hydrogen Energy 2009, 34, 8982.
15. Lee, C. H.; Min, K. A.; Park, H. B.; Hong, Y. T.; Jung, B. O.; Lee, Y. M. J Membr Sci 2007, 303, 258.
16. Wen, S.; Gong, C.; Tsen, W. C.; Shu, Y. C.; Tsai, F. C. J Appl Polym Sci 2010, 116, 1491.
17. Zhang, G.; Zhou, Z. J Membr Sci 2005, 261, 107.
18. Ruffmann, B.; Silva, H.; Schulte, B.; Nunes, S. P.; Solid State Ionics 2003, 162/163, 269.
19. Wang, Z.; Ni, H.; Zhao, C.; Li, X.; Fu, T.; Na, H. J. Polym Sci Part B: Polym Phys 2006, 44, 1967.
20. Zhang, H.; Zhu, B.; Xu, Y. Solid State Ionics 2006, 177, 1123.
21. Ramani, V.; Kunz, H. R.; Fenton, J. M. J Membr Sci 2004, 232, 31.
22. Staiti, P.; Aricò, A. S.; Baglio, V.; Lufrano, F.; Passalacqua, E.; Antonucci, V. Solid State Ionics 2001, 145, 101.
23. Shao, Z.; Joghee, P.; Hsing, I. J Membr Sci 2004, 229, 43.
24. Kim, Y. S.; Wang, F.; Hickner, M.; Zawodzinski, T. A.; McGrath, J. E. J Membr Sci 2003, 212, 263.
25. Sliva, R. F.; Passerini, S.; Pozio, A. Electrochim Acta 2005, 50, 2639.
26. Bradley, W. F. Am Miner 1940, 25, 405.
27. Shen, L.; Lin, Y.; Du, Q.; Zhong, W.; Yang, Y. Polymer 2005, 46, 5758.
28. Wang, L.; Sheng, J. Polymer 2005, 46, 6243.
29. Dai, H.; Guan, R.; Li, C.; Liu, J. Solid State Ionics 2007, 178, 339.

30. Wang, Z.; Ni, H.; Zhao, C.; Li, X.; Fu, T.; Na, H. J Polym Sci Part B: Polym Phys 2006, 44, 1967.
31. Choi, J. K.; Lee, D. K.; Kim, Y. W.; Min, B. R.; Kim, J. H. J Polym Sci Part B: Polym Phys 2008, 46, 691.
32. Shu, Y. C.; Chuang, F. S.; Tsen, W. T.; Chow, J. D.; Gong, C.; Wen, S. J Appl Polym Sci 2008, 108, 1783.
33. Ma, Y. H.; Fang, W. M.; Ma, X. J Mater Rev 2006, 20, 43.
34. Frost, R. L.; Ding, Z. Thermochim Acta 2003, 397, 119.
35. Guan, R.; Dai, H.; Li, C.; Liu, J.; Xu, J. J Membr Sci 2006, 277, 148.
36. Xing, P.; Robertson, G. P.; Guiver, M. D.; Mikhailenko, S. D.; Kaliaguine, S. Macromolecules 2004, 37, 7960.
37. Liu, B.; Robertson, G. P.; Kim, D. S.; Guiver, M. D.; Hu, W.; Jiang, Z. Macromolecules 2007, 40, 1934.
38. Hickner, M. A.; Ghassemi, H.; Kim, Y. S.; Einsla, B. R.; McGrath, J. E. Chem Rev 2004, 104, 4587.